J. Fluid Mech. (1996), *vol.* 308, *pp.* 289–311

Entrainment into two-dimensional and axisymmetric turbulent gravity currents

By MARK A. HALLWORTH[1], HERBERT E. HUPPERT[1], JEREMY C. PHILLIPS[2] AND R. STEPHEN J. SPARKS[2]

[1]Institute of Theoretical Geophysics, Department of Applied Mathematics and Theoretical Physics, University of Cambridge, 20 Silver Street, Cambridge CB3 9EW, UK

[2]Department of Geology, University of Bristol, Bristol BS8 1RJ, UK

(Received 6 June 1995 and in revised form 9 October 1995)

Entrainment of ambient fluid into both two-dimensional and axisymmetric gravity currents is investigated experimentally using a novel neutralization technique. The technique involves the titrative neutralization of an alkaline gravity current which intrudes into and entrains an acidic ambient, and is visualized using a pH indicator solution. Using this technique, we can determine quantitative results for the amount of dilution in the head of the current. The head of the current is able to entrain ambient fluid both by shear instabilities on the current/ambient interface and by over-riding (relatively light) ambient fluid. Guided by our experimental observations, we present two slightly different theoretical models to determine the entrainment into the head of the current as a function of distance from the source for the instantaneous release of a constant volume of fluid in a two-dimensional geometry. By dimensional analysis, we determine from both models that the dimensionless entrainment or dilution ratio, E, defined as the ratio of the volumes of ambient and original fluid in the head, is independent of the initial reduced gravity of the current; and this result is confirmed by our experiments in Boussinesq situations. Our theoretical evaluation of E in terms of the initial cross-sectional area of the current agrees very well with our experimental measurements on the incorporation of an entrainment coefficient α, evaluated experimentally to be 0.063 ± 0.003. We also obtain experimental results for constant-volume gravity currents moving over horizontal surfaces of varying roughness. A particularly surprising result from all the experiments, which is reflected in the theoretical models, is that the head remains essentially unmixed – the entrainment is negligible – in the slumping phase. Thus the heads of gravity currents with identical initial cross-sectional areas but different initial aspect ratios (lock lengths) will begin to be diluted by ambient fluid at different positions and hence propagate at different rates. A range of similar results is determined, both theoretically and experimentally, for the instantaneous release of a fixed volume of (heavy) fluid in an axisymmetric geometry. By contrast, the results of our experiments with gravity currents fed by a constant flux exhibit markedly different entrainment dynamics due to the continual replenishment of the fluid in the head by the constant input of undiluted fluid from the tail.

1. Introduction

Gravity currents occur whenever fluid of one density intrudes primarily horizontally into fluid of a different density. The density contrast may be due to differences

in temperature, composition or bulk properties of particle suspensions, and representative examples of all these situations are found frequently in nature. For instance, many mesoscale meteorological phenomena such as katabatic winds and sea-breezes are gravity currents driven by thermally controlled density differences between adjacent air masses. Differences in salinity account for the spreading of fresh river water above seawater in estuarine environments, whilst the horizontal intrusion of volcanic eruption columns at their neutral buoyancy level in the stratosphere and the flow of sediment-laden turbidity currents along the ocean floors provide natural examples of particle suspension currents. Laboratory modelling of gravity currents has elucidated many features of their dynamics on larger scales. A comprehensive and informative review of such modelling and its application to the environment is contained in Simpson (1987).

Gravity currents are driven by the excess buoyancy between the intruding fluid and the ambient. They can propagate at high Reynolds number (typically greater than 10^3), when the buoyancy forces are balanced by inertial forces, at low Reynolds number (typically less than 10), when the buoyancy forces are balanced by viscous forces, or at intermediate Reynolds number, which is the least-investigated, but also least-frequent, regime.

Gravity currents that flow at high Reynolds number are unsteady and turbulent, and tend to entrain ambient fluid. The consequences of such entrainment, and the resulting dilution of the original intruding fluid, can be quite important. For example, many industrial pollutants are discharged into the atmosphere or hydrosphere with a contrasting density to their ambient surroundings. The dilution with distance of any resulting gravity currents by entrainment has important implications for toxicity levels and the degree and extent of contamination. Although the importance of entrainment has been known for quite some time, very little quantitative work has been devoted to this topic. The research reported in this paper aims to redress this imbalance and greatly augment an earlier, preliminary report (Hallworth *et al.* 1993).

The propagation of turbulent gravity currents was first investigated quantitatively by von Kármán (1940), who argued that the depth, h, and the forward velocity, u, of an inviscid, relatively heavy, two-dimensional, Boussinesq gravity current propagating along a horizontal surface into an otherwise quiescent ambient fluid would be related by

$$Fr \equiv u/(g'h)^{1/2} = \sqrt{2}, \tag{1.1a,b}$$

where Fr is the (dimensionless) Froude number of the current and

$$g' = g\Delta\rho/\rho, \tag{1.2}$$

is the reduced gravity, where g is the gravitational acceleration and $\Delta\rho$ is the excess in density of the current over the density of the ambient, ρ. In a later paper Benjamin (1968) showed that von Kármán used Bernoulli's theorem inappropriately, but nevertheless a rigorous approach led to the identical condition (1.1). Subsequent laboratory experiments by Huppert & Simpson (1980) indicated that in reality (1.1) should be replaced by

$$Fr = 1.19 \tag{1.3}$$

for the situation where the ambient fluid is very much deeper than the intruding current. The smaller Froude number in a real fluid represents the extra retarding effects due to Reynolds stresses and viscous drag at the head of the current, as discussed further by Bonnecaze, Huppert & Lister (1993).

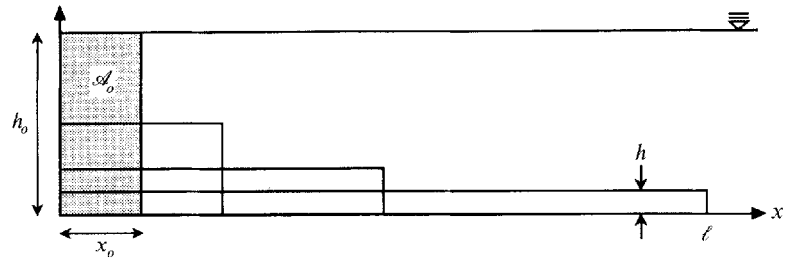

FIGURE 1. Diagram depicting the box-model collapse of a two-dimensional gravity current of initial volume $\mathscr{A}_o$ through a series of rectangles of equal cross-sectional area.

The conditions (1.1) or (1.3) represent but one relationship between two unknowns – the depth h and the velocity u. Another relationship between these two variables is required to close the problem, and this relationship is dependent upon whether the gravity current is the result of the instantaneous release of a fixed volume of fluid or the continuous release of fluid with possibly a time-dependent flux. For the fixed-volume case, a simple, but powerful, analysis can be made by considering the current to take the shape of a series of *non-entraining* rectangles or boxes of constant cross-sectional area $\mathscr{A}$ (Huppert & Simpson 1980), as sketched in figure 1. Denoting the length of the current by ℓ, and equating $\mathrm{d}\ell/\mathrm{d}t$ with u, we thus obtain the two equations

$$h\,\ell = \mathscr{A} \qquad \text{and} \qquad \frac{\mathrm{d}\ell}{\mathrm{d}t} = Fr(g'h)^{1/2}. \tag{1.4a,b}$$

Inserting (1.4*a*) into (1.4*b*) and integrating the result with the assumption that the current initially has zero length, we obtain the relationship

$$\ell = (1.5\ Fr)^{2/3}(g'\mathscr{A})^{1/3}t^{2/3}. \tag{1.5}$$

Rigorous solution of the inviscid Euler equations (Fannelop & Waldman 1972; Hoult 1972; Chen 1980; Bonnecaze *et al.* 1993) leads to a long-term similarity solution which yields relationships for h and u as functions of the downstream coordinate x. The horizontal extent of the current is the same as that given by (1.5) except that the pre-multiplicative function of Fr is slightly altered. The similarity solution sets in after an initiation or 'slumping' phase (Huppert & Simpson 1980) during which time a bore travels back from the front of the current, reflects off the back wall and catches up with the head (Rottman & Simpson 1983; Bonnecaze *et al.* 1993). During this time the current propagates at a fairly constant velocity and travels a distance known as the slumping distance, x_s, which has been determined empirically to be given by (Rottman & Simpson 1983)

$$x_s/x_o = 3 + 7.4h_o/H, \tag{1.6}$$

where x_o is the length of the lock, h_o is the initial height of the fluid behind the lock gate and H is the total depth of ambient fluid.

The theoretical prediction (1.5) is in excellent agreement with experimental results from many different studies (see, for example, Simpson 1987 or Bonnecaze *et al.* 1993 and references therein) even though the theory neglects any effects of entrainment, which must presumably have been present in all the experiments. Part of the reason for this agreement is that the variables g' and $\mathscr{A}$ only appear in (1.5) as the product $g'\mathscr{A}$, and if any ambient fluid is entrained uniformly into the gravity current it increases the cross-sectional area and decreases the reduced gravity in such a way that buoyancy is conserved and $g'\mathscr{A}$ remains constant. On the other hand, however, the entrainment

induces a drag on the current, which must slow it down in comparison with the two-thirds formula of (1.5). Part of the aim of the present work is to evaluate each of the two contributions g' and $\mathscr{A}$ separately, as well as the actual rate of propagation of the current.

A novel experimental approach to measure quantitatively the amount of entrainment into a gravity current is presented in §2. The technique relies on the titrative neutralization of an alkaline gravity current by entrainment of acidic ambient fluid. Related, but different techniques involving chemical reactions have been used to study mixing in turbulent jets, thermals and wakes (see, for example, Breidenthal 1981; Koochesfahani & Dimotakis 1986 and Johari 1992). The neutralization point is visualized by using a universal pH indicator solution which exhibits identifiable colour changes from purple (pH $>$ 10) through green (pH $=$ 7) to red (pH $<$ 4). From a series of experiments with different initial ratios of acid to base, the degree of entrainment into the head of a gravity current can be evaluated as a function of its length. The results of such measurements act as a guide to the theoretical development presented in §3. That section concentrates on the two-dimensional currents that ensue from the instantaneous release of a fixed volume of fluid. The style and degree of entrainment is discussed for currents propagating over either a smooth or a rough horizontal bottom, or below a free surface. The entrainment into axisymmetric, fixed-volume currents is considered in §4. Currents due to a continuous flux are discussed in §5 and it is shown that the result of the entrainment in this case is quite different and much more difficult to quantify. A series of conclusions and some indication of how our quantitative concepts can be applied to natural and industrial situations is presented in the final section. We also quantify there the relative contribution of different entrainment processes to the overall dilution, and discuss the importance of different initial aspect ratios on the subsequent evolution of the current.

2. The experimental technique

A number of different channels of rectangular cross-section, all with horizontal floors, were used for the experiments. For each experiment the channel was filled to the desired height, H, with tap water and a vertical lock gate was inserted at the desired distance, x_o, from one end of the tank (figure 2*a*). Known amounts of salt, sodium hydroxide (NaOH) solution and some universal pH indicator were then added to the water behind the lock to produce the desired density excess and turn the final alkaline mixture purple (pH $>$ 10). The ambient fluid ahead of the gate was acidified using sufficient hydrochloric acid to achieve a pH of less than 4. For some experiments the depth of saline solution behind the lock, h_o, was (considerably) less than the depth of the ambient H, and so, after the addition of the NaOH and pH indicator to this solution, fresh water was carefully floated on top of it to make up a total depth behind the lock of H. In order to produce light gravity currents flowing below the free surface, salt was added to the acidified ambient fluid rather than behind the lock.

After all fluid disturbances had died away, the lock gate was raised out of the fluid and the ensuing alkaline gravity current entered the slumping phase depicted schematically in figure 2(*b*,*c*). As it progressed, considerable mixing occurred at the interface between the two fluids through Kelvin–Helmholtz instability, in which waves made up of fluid from the current entrap ambient fluid, a fundamental situation discussed by Corcos & Sherman (1976, 1984) and references therein. This process

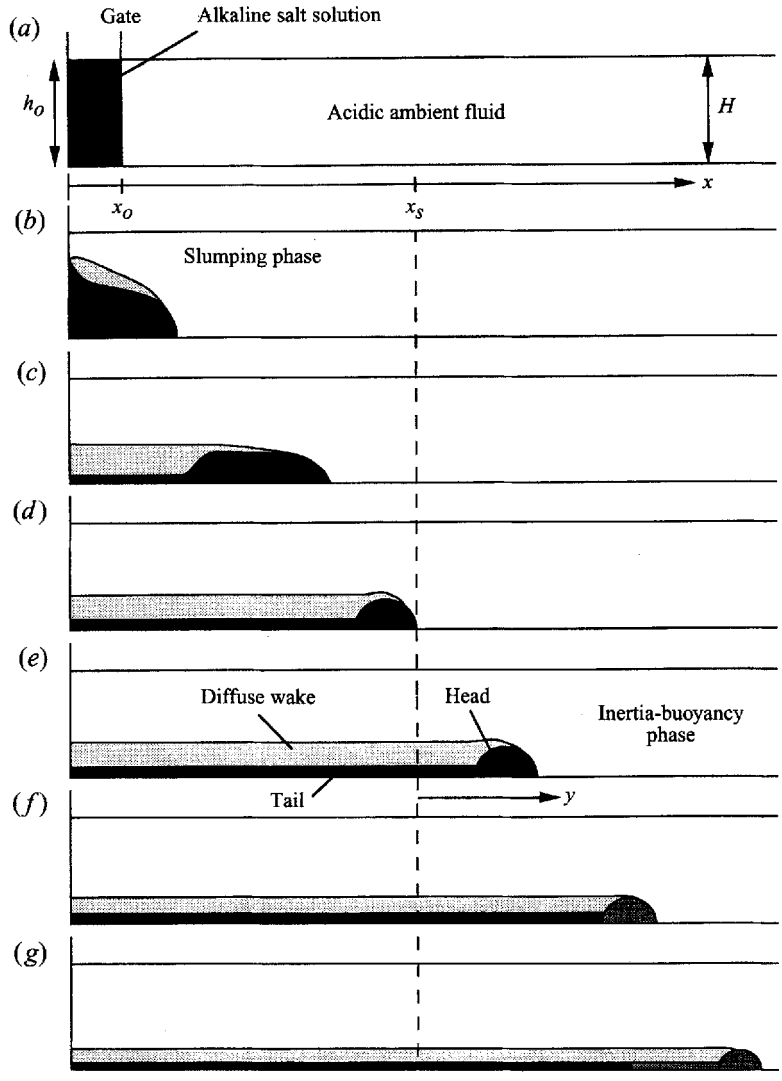

FIGURE 2. Schematic sequence showing the developing stages following the instantaneous release of a two-dimensional, constant-volume alkaline gravity current into an acidified, less-dense ambient fluid. (*a*) Initial configuration; (*b,c*) collapse and shortening of the head within the slumping phase; (*d*) well-formed head at the slumping distance x_s; (*e*) typical flow profile within the inertia-buoyancy regime; (*f*) neutralization of the head by entrainment of sufficient acidic ambient fluid; (*g*) further downstream advance, showing the reduction in the volume of the head as fluid is detrained into the tail and diffuse wake, and the effective 'freezing-in' of the neutralization point in the tail.

was evident from the formation of a diffuse, red envelope of acidified fluid streaming off the upper surface of the advancing, unmixed purple current below, which left behind a diffuse mixed wake. Undiluted, purple fluid was also laid down behind the advancing head in a thin tail layer. Both the trailing tail and overlying wake displayed only weak residual forward motion.

At the slumping distance (figure 2*d*), the reflected bore had effectively caught up with the front of the current, the head having been progressively reduced in length into its characteristic inertial form of approximately semicircular cross-section. Thereafter, even though the head was continually entraining ambient fluid, the volume of the

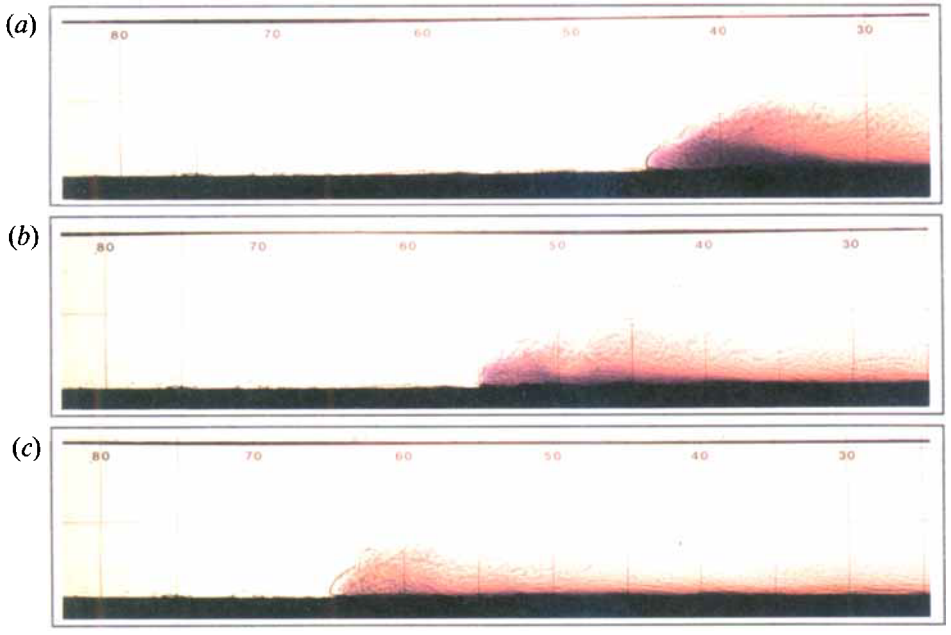

FIGURE 3. Photographs of a two-dimensional gravity current formed by the instantaneous release of a fixed volume of alkaline salt solution containing pH indicator into an acidified freshwater ambient environment. Initial conditions: $A_o = 65$ cm^2, $x_o = 5.0$ cm, $h_o = H = 11.3$ cm and $g'_o = 20$ cm s^{-2}. (*a*) Slumping phase; (*b*) inertia-buoyancy phase; (*c*) the head at the position of neutralization.

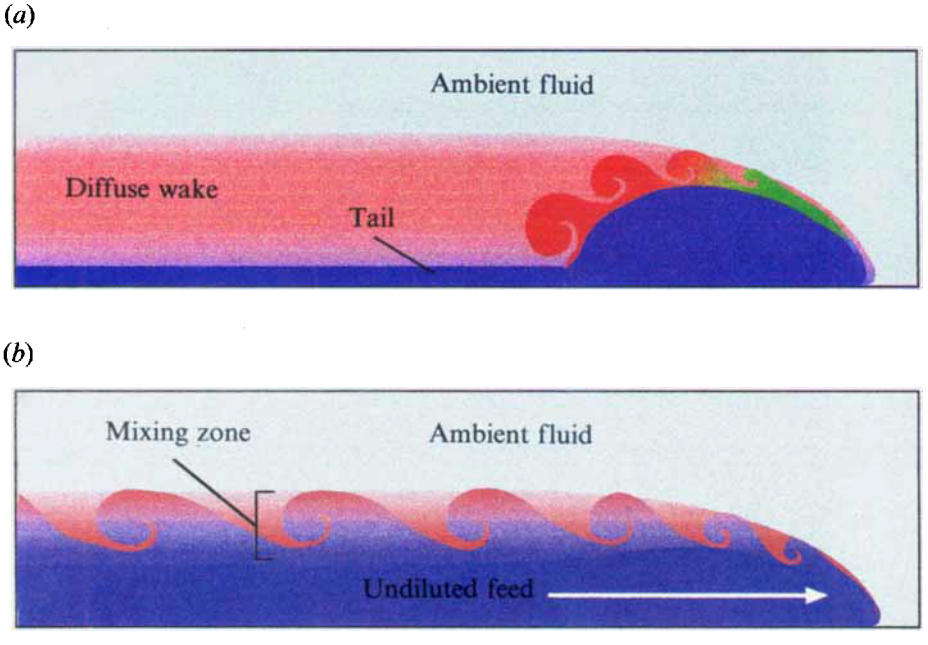

FIGURE 12. Schematic comparison between entrainment mechanisms and regions for (*a*) constant-volume, and (*b*) constant-flux gravity currents.

head decreased monotonically with downstream distance due to mixed fluid being left behind in the tail (figure 2*e–g*). Note that in this regime the form of entrainment is quite different from that envisaged for a vertically rising buoyant plume, for which the entrainment from the ambient takes place along the entire length of the plume, as first described in the famous paper by Morton, Taylor & Turner (1956) and reviewed recently by Turner (1986).

In currents generated by an instantaneous release, turbulent mixing within the head was vigorous and the concentration of salt, and base, in the head was fairly uniform. Beyond the slumping distance, our measurements of the length of the current as a function of time agreed well with the prediction (1.5). At a specific distance downstream, which we could measure to within about ± 1 cm, sufficient acidified ambient fluid had been entrained into the head to neutralize the NaOH present (figure 2*f*). This point, which was dependent on the initial concentration of NaOH, was easily identified because it coincided with an abrupt, homogeneous change in colour of the pH indicator from purple to red throughout the whole head. A series of photographs depicting this transition is shown in figure 3. Beyond the position of neutrality, the head continued to advance, but thereafter the passive tail left behind was also red (figure 2*g*). The transition point was therefore effectively 'frozen-in' to the tail, and only slowly migrated downstream a few centimetres due to weak residual forward motion in the tail.

A number of experimental series were performed with systematic variation of the initial conditions g'_o, x_o, h_o and H, as presented in table 1. Typical values of the Reynolds number at the transition point were between 10^3 and 10^4. Within each series, several experimental runs were conducted, with each particular run having a different initial concentration of NaOH, but otherwise identical initial conditions. Titration of a sample of acidic ambient against a sample of the initial alkaline current before each run led to the determination of the volumetric mixing ratio of the two fluids necessary to achieve neutralization. The experiment itself then yielded the distance along the tank at which the neutralization occurred. In this way it was possible to map out the volumetric proportion of ambient fluid entrained into the gravity current as a function of distance from the source.

3. Two-dimensional, constant-volume currents

In order to quantify the experimental results, we denote by E the dimensionless entrainment ratio as defined by

$$E = A_a/A_b, \tag{3.1}$$

where A_a and A_b are the volumes of acidic ambient and original basic fluid per unit width in the head respectively. The value of E will initially be zero (because there is not yet any entrainment) and tends to infinity with increasing proportion of entrained fluid. Figure 4 presents measurements of E as a function of x, the distance downstream from the back of the gate, for a range of different initial conditions including three different lock lengths, x_o. For some distance there is virtually no entrainment into the head. Beyond this distance, E increases significantly downstream. From the data we can equate the beginning of the significant mixing phase with the slumping distance, x_s (1.6). For experiments with the same lock length, x_o, the value of E at a fixed value of x decreases monotonically with increasing inital volume of fluid behind the gate.

A systematic collapse of all these data can be obtained by dimensional analysis. We denote by A_0 the initial cross-sectional area, or volume per unit width, of the

(a)

Series	x_o (cm)	h_o (cm)	H (cm)	x_s (cm)	A_o (cm^2)	g'_o (cm s^{-2})
A (s)	5.0	9.3	9.3	52.0	46.5	20.0
B (s)	2.5	9.3	9.3	26.0	23.3	20.0
C (s)	5.0	6.0	6.0	52.0	30.0	20.0
D (s)	5.0	13.5	13.5	52.0	67.5	20.0
E (s)	10.0	5.0	40.0	39.2	50.0	18.7
F (s)	10.0	5.0	35.0	40.6	50.0	37.3
G (s)	10.0	5.0	30.0	42.3	50.0	10.3
H (s)	10.0	6.5	6.5	104.0	65.0	20.3
I (s)	10.0	13.0	13.0	104.0	130.0	20.3
J (s)	10.0	23.0	23.0	104.0	230.0	20.3
K (s)	5.3	10.0	10.0	55.0	53.0	10.0
L (s)	5.3	10.0	10.0	55.0	53.0	20.0
M (s)	5.3	10.0	10.0	55.0	53.0	40.0
N (s)	5.3	10.0	10.0	55.0	53.0	80.0
O (r)	5.3	10.0	10.0	55.1	53.0	20.0
P (r)	5.3	10.0	10.0	55.1	53.0	40.0
Q (f)	5.3	10.0	10.0	55.1	53.0	20.0

(b)

Series	r_o (cm)	h_o (cm)	H (cm)	r_s (cm)	V_o (cm^3)	g'_o (cm s^{-2})
R (s)	30.0	10.0	10.0	90.0	28274	20.0
S (s)	30.0	10.0	10.0	90.0	28274	10.0
T (s)	30.0	10.0	10.0	90.0	28274	40.0
U (s)	30.0	10.0	10.0	90.0	28274	80.0
V (s)	30.0	20.0	20.0	90.0	56549	20.0
W (s)	42.4	10.0	10.0	127.2	56478	20.0
X (s)	60.0	10.0	10.0	180.0	113097	20.0

TABLE 1. Initial conditions of the experimental gravity currents for instantaneous constant-volume release in (*a*) two-dimensional and (*b*) axisymmetric geometries. Flows over a smooth floor, roughened floor and at a free surface are denoted by (s), (r) and (f) respectively. The two-dimensional experiments were conducted in a channel of width $W = 29.1$ cm, apart from Series E, F, G, I and J, where $W = 20.8$ cm.

intruding fluid. Dimensional arguments in this Boussinesq situation, guided by the variables in (1.5), then suggest the hypothesis that the proportion of ambient fluid entrained into the gravity current head will depend on: A_o, of dimension L^2; the initial reduced gravity $g'_o = g\Delta\rho/\rho$, of dimension LT^{-2}; and the length of the gravity current x, of dimension L; and possibly non-dimensional shape factors like x_o/h_o, the aspect ratio, and h_o/H, the relative depth of the initial configuration. Because E is dimensionless, it is seen immediately that it must be independent of g'_o, the only external parameter dependent on T. This conclusion was verified by the results of experiments at different values of g'_o, all of which collapse onto the same curve of E against x, as shown in figure 5. Turning this argument around, the collapse shows that some other variable that is dependent upon T cannot play a fundamental role in the entrainment process. In particular, the kinematic viscosity ν, of dimension L^2T^{-1}, cannot be important over the range of Reynolds number used here, as might (incorrectly) have been suggested.

For $0 < x < x_s$, $E \approx 0$ which indicates that right to the end of the slumping phase the head remains essentially undiluted. This is a surprising result, given that

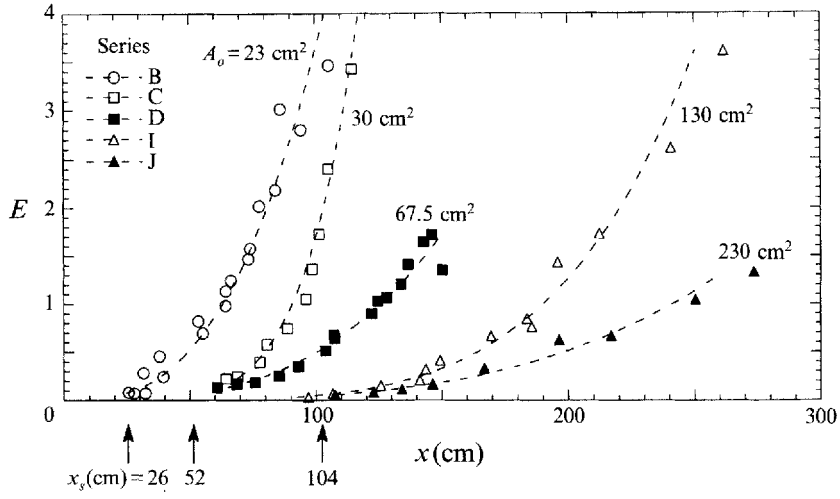

FIGURE 4. Measured entrainment ratio E for the head of a two-dimensional gravity current as a function of distance from the back of the lock. Each point corresponds to a different run within a particular series, the initial conditions for which are presented in table 1. Data shown include series at three different initial lock lengths (with the corresponding slumping distances arrowed) and a range of initial volumes. The error in this and subsequent figures in determining each point is less than the size of the symbol. Smooth curves have been drawn through the data to facilitate visualization of the trend.

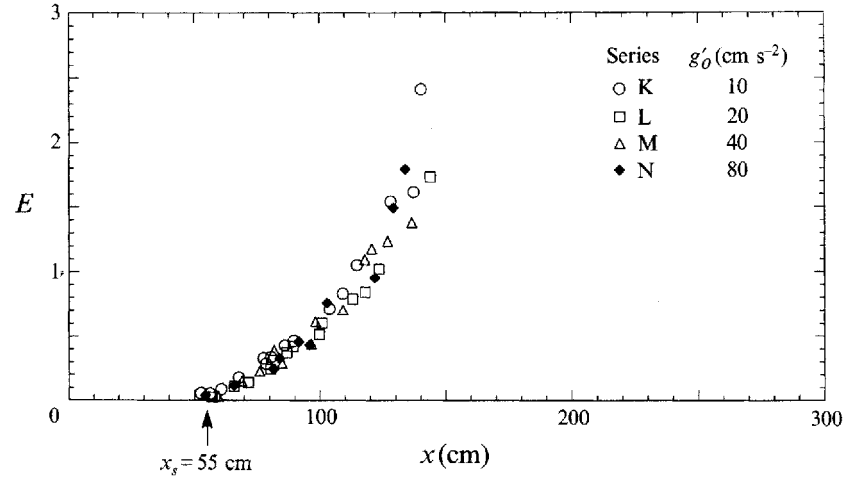

FIGURE 5. Data for four series of experiments with different initial values of g'_o but otherwise identical initial conditions (as given in table 1), presented in the same form as figure 4.

some mixing definitely occurs through shear instabilities at the interface of the gravity current (see figure 2*c*,*d*). Our measurements indicate quite clearly, however, that the mixed fluid does not penetrate into the head. We do not at present have a good physical argument as to why this is so, but it is a definite fact which arises from all our experimental measurements. To accommodate this, we introduce the new variable $y = x - x_s$. Further use of dimensional analysis then indicates that the dimensionless variable E must be a function of $y/A_o^{1/2}$ and the initial shape factors. Replotting all our data in this way we obtain a satisfactory collapse, as shown in figure 6.

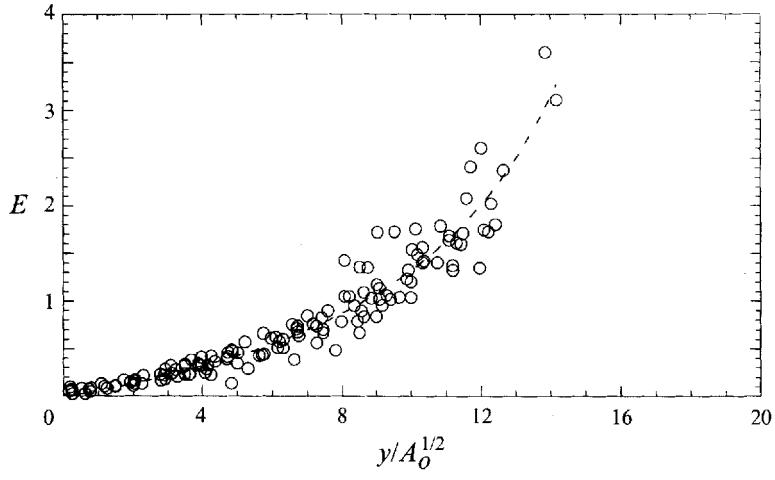

FIGURE 6. Measured entrainment ratio E as a function of $y/A_o^{1/2}$ for all data from two-dimentional constant-volume currents moving over a smooth horizontal solid floor (Series A to N). The dotted line shows a smooth best-fit curve to the data.

The observations can be explained as follows. The cross-sectional area of the head beyond the slumping phase, A, increases by entrainment of ambient fluid into the head and simultaneously decreases by leaving fluid behind in the tail. During the slumping phase, however, no entrainment takes place into the head although fluid is still left behind in the tail. Beyond the slumping distance, consider the infinitesimal change in cross-sectional area of the head, δA, that occurs when the current propagates forward an infinitesimal distance δy. The explicit relationship between these two will be linear and can only depend on A, because any general entrainment law cannot depend on the initial cross-sectional area A_0 or the distance y. Thus, by dimensional analysis, $\delta A \propto A^{1/2}\delta y$, where $A^{1/2}$ represents a characteristic lengthscale for the head. As we discuss further below, the head is observed to have an approximately semi-elliptical cross-section, with a maximum height h being some fraction of $A^{1/2}$. We can hence use the height of the head, defined by

$$h = SA^{1/2}, \tag{3.2}$$

where S is a shape factor, as the relevant lengthscale for entrainment. We will assume that S is constant beyond the slump distance. The most general form accounting for entrainment into the head and the loss of fluid from the head to the tail is then

$$\delta A = (\alpha SA^{1/2} - kSA^{1/2})\delta y, \tag{3.3}$$

where α is an entrainment constant and the constant k reflects the ratio of the height of the tail to that of the head. Taking the limit $\delta y \to 0$, we thus find that

$$\frac{\mathrm{d}A}{\mathrm{d}y} = \alpha SA^{1/2} - kSA^{1/2} \qquad (y > 0). \tag{3.4}$$

The introduction of the shape factor might seem unnecessary, since only the products αS and kS explicitly appear; and the analysis could continue by setting $S = 1$. However, as will be shown later, the shape of the head depends on the roughness of the surface over which the flow moves. By tailoring the value of S to suit a particular surface we afford a means of determining a more generally applicable entrainment constant, rather than deriving different entrainment constants for different surfaces.

To (3.4) we need to add the boundary condition that

$$A = A_s \qquad (y = 0), \tag{3.5}$$

where A_s is the cross-sectional area of the head at the end of the slumping phase.

Our model, as presented so far, does not allow A_s to be evaluated directly. The approach adopted by Hallworth *et al.* (1993), which we herein refer to as model I, was that the amount of fluid left behind in the tail at the end of the slumping phase could be neglected with respect to that in the head at this time, leading to

$$A_s = A_o. \tag{3.6}$$

This approximation is clearly not absolutely correct, because A_s is observed to be significantly less than A_o in our experiments.

An improvement to this first model is to consider the tail at the end of the slumping phase to be a rectangular box of length x_s and height $kS\,A_s^{1/2}$. In this second approach, referred to as model II,

$$A_s = A_o - kSx_sA_s^{1/2}, \tag{3.7}$$

which we can solve as a quadratic for $A_s^{1/2}$ to obtain

$$A_s^{1/2} = \tfrac{1}{2}\left[-kSx_s + \left(k^2S^2x_s^2 + 4A_o\right)^{1/2}\right], \tag{3.8}$$

or

$$A_s = A_o - kSx_s\left[A_o + \tfrac{1}{4}\,k^2S^2x_s^2\right]^{1/2} + \tfrac{1}{2}\,k^2S^2x_s^2. \tag{3.9}$$

This second model does not rely on any processes which occur within the slumping phase; it merely develops an approximation for the volume of the head at the end of this phase in terms of the product of the two constants S and k which appear in (3.4). Indeed, a full description of the slumping phase is too complex to model in detail, in view of the fact that the shape factor S within this phase is far from constant, but varies significantly with y from an initial value of $(h_o/x_o)^{1/2}$ at $y = -x_s$, through the various adjustment stages of collapse and head shortening, to its final steady value at $y = 0$.

Having determined an expression for A_s, we can solve (3.4) with the boundary condition (3.5) to obtain

$$A/A_s = \left[1 + \tfrac{1}{2}S(\alpha - k)y/A_s^{1/2}\right]^2 \qquad (y \geqslant 0). \tag{3.10}$$

Equation (3.10) suggests that the head considered as a separate entity runs out of volume at

$$y = y_c \equiv 2A_s^{1/2}/S(k - \alpha). \tag{3.11}$$

Beyond y_c the fluid in the tail must continue to move slowly forward, driven by horizontal density gradients. In almost (but not absolutely) all natural or laboratory situations, viscous effects dominate before the current has reached $y = y_c$ and (3.10) is no longer valid there.

To determine an expression for E, we need to keep account of the ambient fluid and original fluid individually. Since no entrainment into the head occurs in the slumping phase, the relevant equations, following (3.4), are

$$\frac{\mathrm{d}A_a}{\mathrm{d}y} = \alpha SA^{1/2} - kpSA^{1/2}, \quad \frac{\mathrm{d}A_b}{\mathrm{d}y} = -k(1-p)SA^{1/2}, \tag{3.12a,b}$$

$$A_a(0) = 0, \qquad A_b(0) = A_s, \tag{3.13a,b}$$

	Model I using $S = (2/\pi)^{1/2}$		Model II using $S = (2/\pi)^{1/2}$		Model II using measured S		
	α	k	α	k	S	α	k
2D Smooth floor	0.079	0.195	0.058	0.127	0.71	0.065	0.142
3D Smooth floor	0.089	0.176	0.065	0.128			
2D Rough floor	0.103	0.258	0.064	0.161	0.83	0.062	0.155
2D Free surface	0.021	0.213	0.013	0.140	0.55	0.019	0.203

TABLE 2. Summary of the best-fit values of the entrainment constant α and the tail/head height ratio k in both two-dimensional (2D) and axisymmetric (3D) geometries, evaluated using $S = (2/\pi)^{1/2}$ for model I (where $A_s = A_a$) and model II (where A_s is given by (3.9)). Also presented are the model II results using the directly measured S values.

where $p = A_a/A$ and $1-p = A_b/A$. Equations (3.10), (3.12) and (3.13) represent three consistent equations for two of the unknowns A_a, A_b, and $A = A_a + A_b$. Any two of the equations would suffice, but we present each one because of their different physical interpretation. Substituting the expressions for p, with A represented by (3.10), into (3.12) and (3.13) and integrating the result, we find first that

$$A_b/A_s = \left[1 + \tfrac{1}{2}S(\alpha - k)y/A_s^{1/2}\right]^{2k/(k-\alpha)} \tag{3.14}$$

and then that

$$A_a/A_s = \left[1 + \tfrac{1}{2}S(\alpha - k)y/A_s^{1/2}\right]^{2} - \left[1 + \tfrac{1}{2}S(\alpha - k)y/A_s^{1/2}\right]^{2k/(k-\alpha)}. \tag{3.15}$$

Dividing the right-hand sides of (3.14) and (3.15), as indicated by (3.1), we deduce, after a little re-arrangement, that

$$E = \left[1 + \tfrac{1}{2}S(\alpha - k)y/A_s^{1/2}\right]^{2\alpha/(\alpha-k)} - 1, \tag{3.16}$$

which becomes infinite as $y \to y_c$.

It would now be intellectually most satisfying to evaluate α and k from theoretical arguments. This we cannot do, but are somewhat mollified by the realization that even though the famous Morton *et al.* (1956) model for the entrainment into a turbulent plume was put forward almost 40 years ago, and has been worked on and used extensively since, no purely theoretical calculation for the value of their constant α has been possible – only experimental determinations have been presented. Similarly, we must rest content with experimental determinations of the constants α and k.

The explicit evaluation of α and k themselves from (3.16) relies on choosing a suitable value of the shape factor S for $y > 0$, although only the products αS and kS appear in all the equations. If the cross-sectional shape of the head were an exact semicircle, then (3.2) yields $S = (2/\pi)^{1/2} = 0.798$. However, we observed from our experimental gravity currents moving over a smooth floor, a roughened floor and along a free surface that the shape of the head varies with the frictional drag imposed at the boundary. Analyses of video frames taken of our laboratory runs allowed us to measure mean values of S of 0.71 ± 0.002 and 0.83 ± 0.03 for the smooth floor and roughened floor respectively, which are fairly close to the value for a semicircle. Measurement of a mean S value for the free surface currents proved more problematical because the head in this case was flattened into the form of an extended wedge, the height of which barely exceeded that of the following tail region. It was thus difficult to define a discrete area for the head. However, our rather

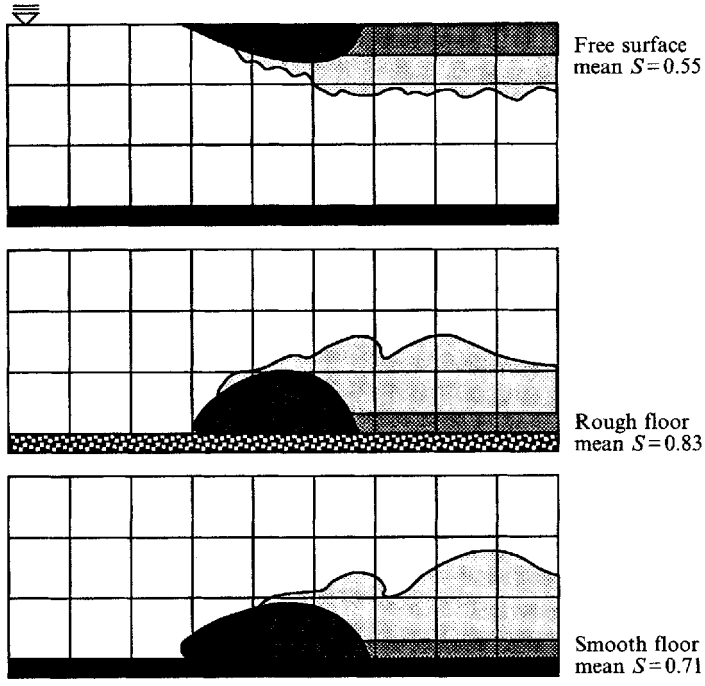

FIGURE 7. Representative tracings reproduced from video frame analyses showing the relative cross-sectional shape of the head (dark stipple) for the three different boundary surfaces.

subjective measurements suggested a mean S value of 0.55 ± 0.03. Representative tracings of the head profiles are depicted in figure 7. Further consideration of the shape factor is deferred for later discussion, and a comparison of the results obtained using different values of S is presented in table 2.

Using the approximation $S = (2/\pi)^{1/2}$ for heavy gravity currents moving over a smooth, horizontal floor, data for all these experiments are presented in figure 8(*a*) as a plot of E against $y/A_s^{1/2}$, where $A_s^{1/2}$ was determined from (3.9) using a k value iteratively matched to that evaluated (along with α) from the curve of least-squares best-fit through the data in the form of (3.16) in the following way. A reasonable initial estimate of k was chosen to evaluate A_s from (3.9), and the functional form of (3.16) was then plotted against the data to determine the resulting best-fit values of α and k. Replotting the data using this improved value of k to evaluate A_s, the curve-fitting was then repeated, and the operations iterated until successive values of k matched to within 1%. This procedure yields $\alpha = 0.058 \pm 0.001$ and $k = 0.127 \pm 0.002$.

The series of experiments for heavy gravity currents over a roughened floor were conducted in a tank whose floor had been covered by a thin layer of granules with a mean grain diameter of ≈ 2 mm. The evaluation procedure described above, again using $S = (2/\pi)^{1/2}$, gave $\alpha = 0.064 \pm 0.004$ and $k = 0.161 \pm 0.001$. The data and appropriate curve are presented in figure 8(*b*). Note that using the alternative approximation (3.6) of Hallworth *et al.* (1993) leads to $\alpha = 0.079$, $k = 0.195$ for the smooth floor case, and $\alpha = 0.103$, $k = 0.258$ for the rough floor.†

† The values reported in Hallworth *et al.* (1993) of $\alpha = 0.078$ and $k = 0.147$ were based on the notation that $S = 1$, and taking measurements from the gate rather than from the back of the lock, since the position of the gate is more relevant to the concepts behind model I.

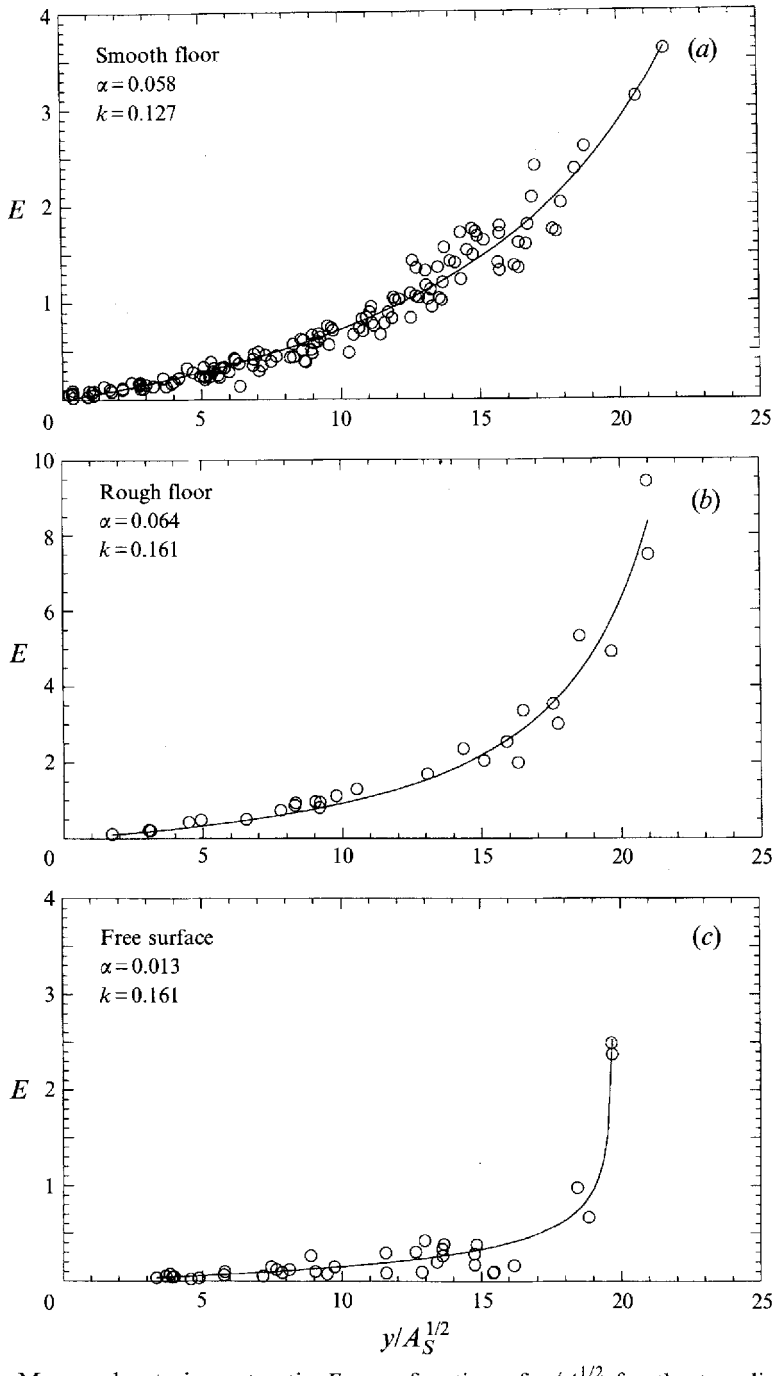

FIGURE 8. Measured entrainment ratio E as a function of $y/A_s^{1/2}$ for the two-dimensional constant-volume currents moving over (*a*) a smooth, rigid surface; (*b*) a roughened, rigid surface; and (*c*) a free surface. Best-fit curves of the form (3.16) are shown in each case (using $S = (2/\pi)^{1/2}$), along with the corresponding evaluated values of α and k.

Our experiments with light gravity currents spreading beneath a free surface were rather inconclusive. It became apparent that entrainment in this situation was much less than in the previous cases, and the length of our tank (150 cm) was only sufficient for relatively small values of E to be measured. The data are thus somewhat ill-conditioned with respect to fitting a curve of the form (3.6), but are nonetheless presented in figure 8(*c*), and yield α and k values of 0.013 ± 0.001 and 0.140 ± 0.001 respectively using the (less appropriate in this case) value of $S = (2/\pi)^{1/2}$. Although the application of our model may not be completely satisfactory for free surface currents, it is undoubtedly clear that the entrainment into such currents is significantly less than that observed for flows over a rigid boundary.

We are now able to evaluate g', $g'A$ and the rate of propagation of the current. From the definitions of A_a and A_b, and the use of (3.10) and (3.14) it follows that

$$g' = g'_o A_b/A = g'_o \left[1 + \tfrac{1}{2}S(\alpha - k)y/A_s^{1/2}\right]^{2\alpha/(k-\alpha)} \tag{3.17a}$$

and

$$g'A = g'_o A_s \left[1 + \tfrac{1}{2}S(\alpha - k)y/A_s^{1/2}\right]^{2k/(k-\alpha)}. \tag{3.17b}$$

To evaluate the rate of propagation of the current we employ the head condition (1.1*a*). Since, from (3.2), (3.10) and (3.17*a*),

$$g'h = g'_o S A_s^{1/2} \left[1 + \tfrac{1}{2}S(\alpha - k)y/A_s^{1/2}\right]^{(k+\alpha)/(k-\alpha)}, \tag{3.18}$$

we can write

$$u \equiv \frac{\mathrm{d}y}{\mathrm{d}t} = Fr(g'_o S)^{1/2} A_s^{1/4} \left[1 + \tfrac{1}{2}S(\alpha - k)y/A_s^{1/2}\right]^{(k+\alpha)/2(k-\alpha)}, \tag{3.19}$$

a differential equation to which must be added the boundary condition

$$y = 0 \qquad (t = t_s), \tag{3.20}$$

where t_s is the time for the initial current to attain the slumping distance x_s. The solution of (3.19) and (3.20), in terms of the non-dimensional distance

$$Y = \tfrac{1}{2}S(k - \alpha)y/A_s^{1/2} \equiv y/y_c \tag{3.21a,b}$$

and non-dimensional time

$$T = Fr(g'_o S)^{1/2} A_s^{1/4} y_c^{-1}(t - t_s) \tag{3.21c}$$

is

$$Y = 1 - \left[1 - \frac{k - 3\alpha}{2(k - \alpha)} T\right]^{2(k-\alpha)/(k-3\alpha)}. \tag{3.22}$$

This relationship does not at first sight look much like the two-thirds similarity form of solution (1.5). However, incorporating $\alpha = 0.058$ and $k = 0.127$, the model II values presented in table 2 for flows over a solid boundary, and plotting (3.22) as done in figure 9, we see that the two are of the same form for a wide range of t. In addition, the curves obtained by using any of the pairs of values in table 2 hardly differ from the one presented. This general agreement helps to explain why predictions based on the similarity solution (1.5), obtained without recourse to the effects of entrainment, are in good agreement with data obtained from real, entraining gravity currents. The agreement also acts as a confirmation that our determinations of α and k are in the appropriate range.

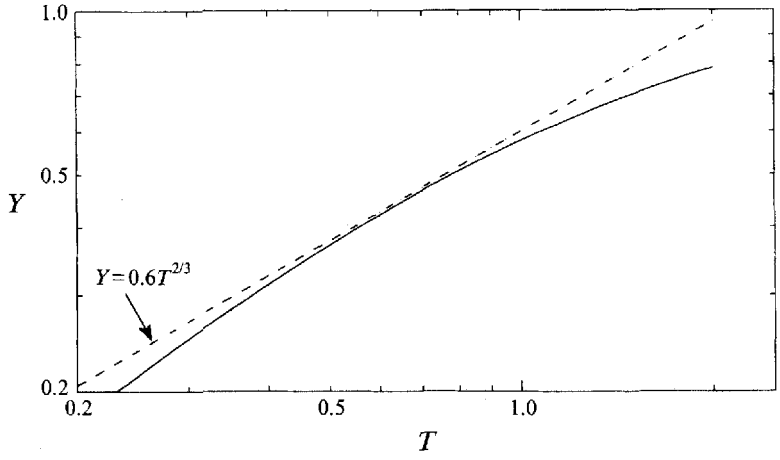

FIGURE 9. Log-log plot of non-dimensional distance Y against non-dimensional time T of the form (3.22), using $\alpha = 0.058$ and $k = 0.127$. The dotted line indicates the two-thirds power law dependence of distance on time according to the similarity solution (1.5).

4. Axisymmetric, constant-volume currents

In this section we concentrate on axisymmetric gravity currents that result from the instantaneous release of a fixed volume of heavy fluid $\mathscr{V}$. Adjusting the argument that lead to (1.4) and (1.5) so as to be applicable to axisymmetric currents, we find that the radius of the current, r, as a function of time is given by

$$r = (4g'\mathscr{V}Fr^2/\pi)^{1/4}\, t^{1/2}. \tag{4.1}$$

The slumping distance, r_s, has been determined only for the situation when the initial depth of the current, h_o, equals that of the ambient fluid, H. Our experiments in this case indicate that

$$r_s/r_o = 3, \tag{4.2}$$

where r_o is the radius of the lock gate.

The derivation of the governing equations in the axisymmetric situation is more subtle than in the two-dimensional case but is guided by it. We seek to determine how the volume V of the axisymmetric gravity current head evolves as the radius of the current increases. It is easier to use the volume of the head, rather than the cross-sectional area, in the axisymmetric case because as the current spreads the volume of the head changes only in response to entrainment and loss of fluid to the tail. In contrast, the cross-sectional area of the head changes additionally due to the geometric effects of radial spreading. As we demonstrated in the two-dimensional case, the spatial rate of both the entrainment and the amount of fluid left behind in the tail per unit width is directly proportional to the height, h, of the head. We assume, as before in (3.2), that the height scales with the cross-sectional area of the head A by $h = SA^{1/2}$, where the shape factor S is again constant beyond the slumping phase. The volume of the head, V, is $2\pi rA$, so

$$h = S\left(\frac{V}{2\pi r}\right)^{1/2}. \tag{4.3}$$

Thus, as the current moves forward an amount δr, the change in volume, δV, due to entrainment and loss of fluid to the tail is directly proportional to the circumference

$2\pi r$, h and δr. With the same definitions of α and k as in the two-dimensional case, the governing equation then becomes

$$\frac{dV}{dr} = (\alpha - k)S(2\pi rV)^{1/2} \quad (r > r_s), \tag{4.4}$$

$$V = V_s \quad (r = r_s), \tag{4.5}$$

where V_s is the volume of the head at the end of the slumping phase.

As before, two different models can be considered to generate V_s from V_o. For model I

$$V_s = V_o. \tag{4.6}$$

For model II

$$V_s = V_o - \pi k S r_s^2 \left(\frac{V_s}{2\pi r_s}\right)^{1/2} \tag{4.7a}$$

$$= V_o - kS\left(\frac{\pi}{2}\right)^{1/2} r_s^{3/2} V_s^{1/2}, \tag{4.7b}$$

which can again be solved as a quadratic in $V_s^{1/2}$ to obtain

$$V_s^{1/2} = \frac{1}{2}\left[-\left(\frac{\pi}{2}\right)^{1/2} k S r_s^{3/2} + \left(\frac{\pi}{2}k^2 S^2 r_s^3 + 4V_o\right)^{1/2}\right], \tag{4.8}$$

or

$$V_s = V_o - \left(\frac{\pi}{2}\right)^{1/2} k S r_s^{3/2}\left[V_o + \frac{\pi}{8}k^2 S^2 r_s^3\right]^{1/2} + \frac{\pi}{4}k^2 S^2 r_s^3. \tag{4.9}$$

We are now in a position to integrate (4.4) and (4.5) to determine that

$$V/V_s = \left[1 + \frac{(2\pi)^{1/2}}{3} S(\alpha - k)(r^{3/2} - r_s^{3/2})/V_s^{1/2}\right]^2 \qquad (r \geqslant r_s). \tag{4.10}$$

Defining F as the axisymmetric generalization of E by

$$F = V_a/V_b, \tag{4.11}$$

where V_a and V_b are the volumes of acidic ambient and original basic fluid in the axisymmetric head respectively and proceeding as before, we find that

$$F = \left[1 + \frac{(2\pi)^{1/2}}{3} S(\alpha - k)\left(r^{3/2} - r_s^{3/2}\right)/V_s^{1/2}\right]^{2\alpha/(\alpha - k)} - 1. \tag{4.12}$$

Seven sets of experiments with different initial values of g_o', $h_o = H$ and the radius of the lock r_o were carried out with heavy gravity currents propagating over the base of a smooth Perspex sector tank of angle 10° and radius 2.3 m. The initial conditions are shown in table 1. Within each set, several experiments were performed with different initial concentrations of alkali in the salt solution behind the lock. Experimental data are presented in figure 10.

The results confirmed that F was independent of g_o', as required by the dimensional arguments presented in the last section and the explicit form of (4.12). All the data for F as a function of $(r^{3/2} - r_s^{3/2})/V_s^{1/2}$ are presented in figure 11 along with the best-fit curve to (4.11). Using $S = (2/\pi)^{1/2}$ as before, and iteratively matching the best fit value of k to that used in evaluating V_s from (4.9) following the procedure outlined in the previous section, we obtain $\alpha = 0.065 \pm 0.002$ and $k = 0.128 \pm 0.001$, which are very similar to those values determined for the two-dimensional situation.

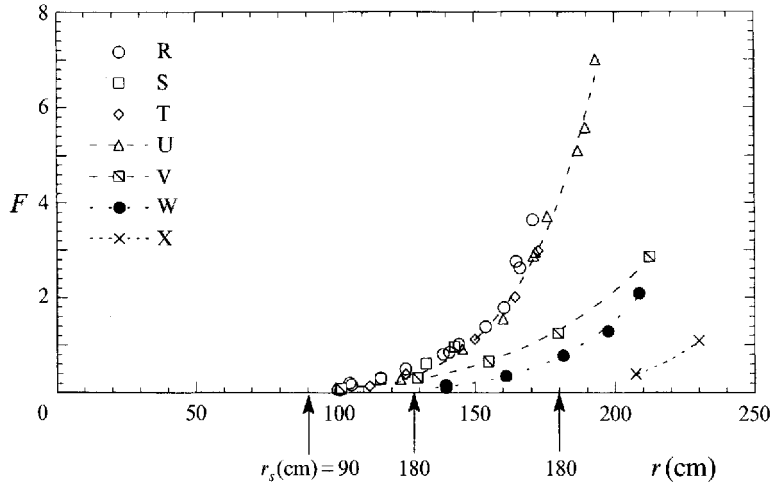

FIGURE 10. Measured entrainment ratio F for the head of axisymmetric constant-volume gravity currents as a function of radius, for experimental series at three different initial lock radii and various initial volumes and density differences. Full initial conditions are given in table 1 (R-X). Slumping distances are arrowed, and smooth curves are drawn through selected data series to aid examination of trends.

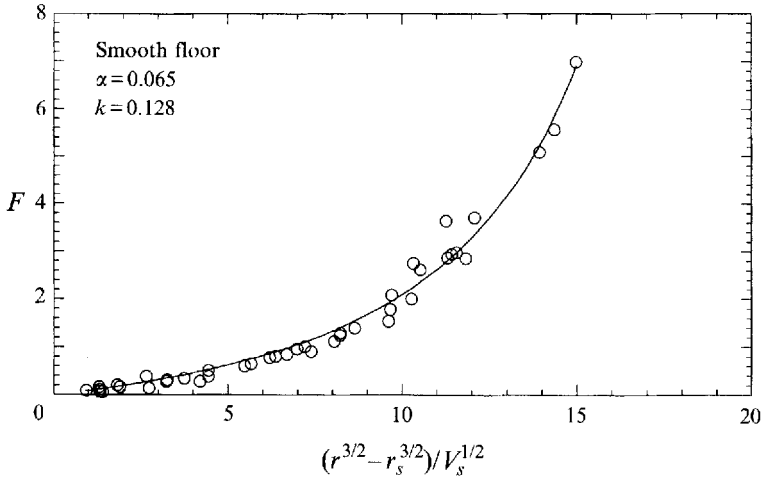

FIGURE 11. Measured entrainment ratio F as a function of $\left(r^{3/2}-r_s^{3/2}\right)/V_s^{1/2}$ for all the axisymmetric constant-volume gravity currents moving over a smooth horizontal surface, with the best-fit theoretical curve in the form of (4.12), and corresponding values of α and k.

5. Constant-flux currents

Our original intention was to apply the neutralization technique to study the entrainment into the head of a gravity current fed at source by a constant input. To this end we designed a flow delivery system for both two-dimensional and axisymmetric fixed-flux currents, and performed a number of sets of experiments in each of the two geometries. From these experiments we conclude that the consequence of the entrainment into the head of a gravity current fed by a constant flux is quite different to that arising from the instantaneous release of a fixed volume of fluid. In contrast to this latter case, there was no abrupt and permanent colour change in the head at

a specific distance. Instead, the fluid in the bulk of the head and in the following tail remained purple at all times although, almost from the source, the head was surrounded by a thin envelope of mixed fluid of greens, reds and purples. This occurred for all the values of g'_o and input flux, which strongly suggests that the result was not due to the constraining effects of the finite length of the tank.

We interpret this difference as being due to the continual replenishment of the fluid in the head by the constant feed of undiluted fluid from the tail. The velocity of this input is approximately 10% larger than that of the head itself, as first documented by Britter & Simpson (1978) and called the overtaking speed by them. We believe that the input from the tail continually combines with the fluid entrained from the ambient and is then left behind as a diffuse wake by the shear instabilities that occur at the head. We conjecture further that a similar process operates during the slumping phase of an instantaneous release of a finite volume of fluid, during which our measurements suggested that there was no entrainment into the head. A schematic sketch contrasting these different styles of entraining behaviour is shown in figure 12 (see p. 294).

6. Discussion and conclusions

A summary of our determined values of α and k for both two-dimensional and axisymmetric constant-volume-release currents is presented in table 2. The results obtained using model I, in which the volume of the head at the end of the slumping phase is equated directly to the initial volume, display fairly large variations in both α and k for the different situations. The values obtained using model II are always lower than those of model I, and for the solid boundary cases display greater self-consistency. The α values determined for the free surface currents are roughly 1/4 those for flows over solid boundaries in both models.

The model II results presented in table 2 were computed either using an S value of $(2/\pi)^{1/2}$, equivalent to approximating the cross-sectional shape of the head to a semicircle, or using the direct measurements of S made from our experiments. It is noticeable that using the directly measured S values serves to tighten the agreement between values of α for the different solid boundary cases. The flow over a roughened floor still displays a marginally higher value of k than for flows over smooth floors, but this only implies an increased tail thickness relative to the head for the rough floor case, which is physically reasonable in terms of basal shear-generated turbulence, and is consistent with the higher S value measured for this case.

Using the directly measured S value of 0.55 for the free surface currents, the best-fit values of α and k are increased to 0.019 and 0.203 respectively, but the entrainment coefficient still remains approximately one-third that of the mean value for flows over a solid floor. We remarked earlier, however, that our measured value here is questionable due to the highly subjective nature of defining a discrete head region for this no-slip situation. To achieve an entrainment coefficient of approximately 0.063 consistent with the solid boundary cases would require values of S and k of 0.156 and 0.715 respectively. While this is reasonable for the value of k (the height of the head is observed to be only slightly greater than that of the ensuing tail for these flows), it would require the cross-sectional shape of the head to be some 50 times longer than it is high, which questions the existence of a discrete head at all. We offer two possible explanations for this behaviour: either the head region by our definition does not exist for free surface flows, or the mechanism of entrainment is dramatically different for this rather special free-slip boundary condition. We prefer this latter explanation on the following grounds.

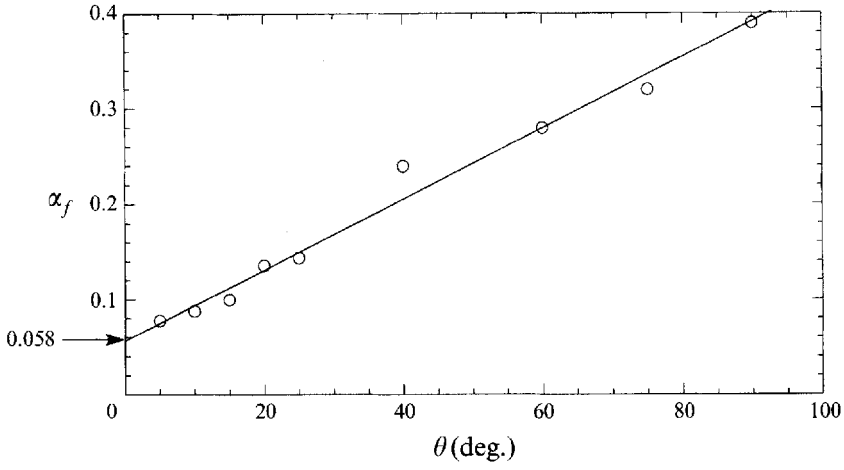

FIGURE 13. Data of Beghin *et al.* (1981) showing the linear variation of α with slope angle (θ) in the range $5° \leqslant \theta < 90°$ for inclined thermals. The best straight line fit through the data gives an extrapolated intercept of $\alpha = 0.058$ for the horizontal situation.

Entrainment has previously been attributed to both mixing through Kelvin–Helmholtz instabilities along the upper surface of the head, and to over-riding and engulfment of ambient fluid in billows and clefts beneath the nose of the head (Britter & Simpson 1978). For free surface currents with theoretically zero basal shear, the over-riding mechanism may not contribute to the overall entrainment of ambient fluid at all, thus yielding a lower overall entrainment coefficient. Comparing the values of α of 0.065 and 0.019, determined using the measured values of S for a smooth floor and a free surface respectively (table 2), we imply that the over-riding mechanism accounts for approximately two-thirds of the total entrainment into the head for flows over a rigid surface.

The consistency of the model II results and its physically more realistic description of real flows are clearly preferable to the approach of model I. For flows over a rigid surface we determine experimentally a mean entrainment coefficient of 0.063 ± 0.003, with the ratio for the height of the tail to the height of the head $k \approx 1/7$. We point out here that by our definition, the tail includes all fluid left behind the head, and treats it as a vertically homogeneous single layer. In reality, this fluid is observed to exhibit a vertical compositional gradient, comprising a thin lower dense tail region overlain by a much thicker, diffuse lower density wake.

Our mean value of α compares favourably with previous experimental determinations of the entrainment coefficient for buoyancy-driven flows. Beghin, Hopfinger & Britter (1981) describe experiments investigating entrainment into two-dimensional thermals moving along inclined, smooth, rigid boundaries, and evaluate values of α which vary linearly with slope angle θ over the range $5° \leqslant \theta < 90°$. Extrapolation of their results to the horizontal situation yields an entrainment coefficient of 0.058 (figure 13), which is gratifyingly similar to our reported value. Fischer *et al.* (1979) report experimentally determined entrainment coefficients of 0.054 and 0.083 for turbulent jets and plumes respectively. While these situations are quite different to the behaviour of turbulent gravity currents moving over a rigid boundary, they serve to illustrate general agreement for the entrainment constant.

Our experiments indicate that entrainment into gravity currents is spatially non-

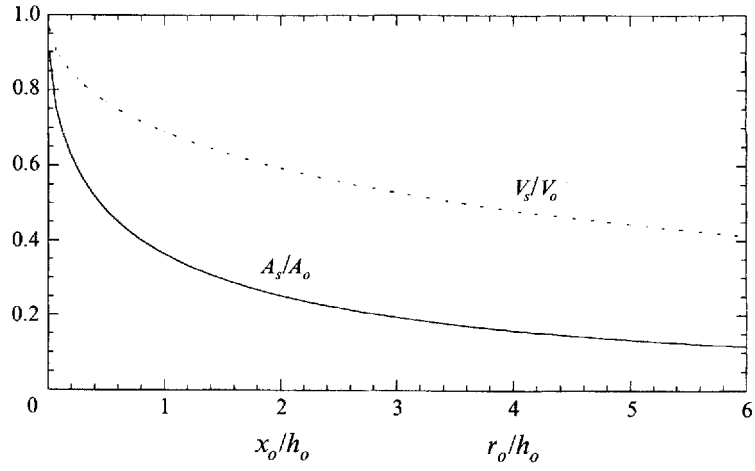

FIGURE 14. Ratio of the volume of the head at the end of the slumping phase to its initial volume plotted as a function of the initial length to height ratio of the released volume, for both two-dimensional and axisymmetric gravity currents.

uniform, and occurs predominantly into the head of the flow, as opposed to being uniform along its full length as envisaged for turbulent plumes. The point at which the head begins to entrain fluid has considerable implications for mixing and dilution with distance, as outlined below.

Our theoretical model (3.16) predicts the composition of the head E at a given distance y beyond the end of the slumping phase as a function of the volume of the head at the end of the slumping phase A_s, where A_s is given by (3.9). Dividing both sides of (3.9) by $A_o = x_o h_o$, and setting $x_s = 10.4x_o$ (for $h = H$), we arrive at the ratio

$$\frac{A_s}{A_o} = 1 - \frac{\beta}{2}\left(\frac{x_o}{h_o}\right)\left[\left(\beta^2 + 4\frac{h_o}{x_o}\right)^{1/2} - \beta\right], \tag{6.1}$$

where $\beta = 10.4kS$.

Similarly, for the axisymmetric case using $V_o = 2\pi r_o^2 h_o$ and (4.2), we find that

$$\frac{V_s}{V_o} = 1 - \frac{\gamma}{2\pi}\left(\frac{r_o}{h_o}\right)\left[\left(\gamma^2 + 4\frac{h_o}{r_o}\right)^{1/2} - \gamma\right], \tag{6.2}$$

where $\gamma = 3(3kS/2\pi)^{1/2}$.

In both cases, the volume of the head at the end of the slumping phase as a fraction of the initial volume is seen to be a function of the initial aspect ratio (x_o/h_o, or r_o/h_o) of the released volume, as plotted in figure 14. Since subsequent entrainment into the head depends on A_s (or V_s), variation in the initial aspect ratio can greatly influence the resulting dilution with distance.

For example, an initially low aspect ratio flow (x_o/h_o or $r_o/h_o \ll 1$) delivers a relatively large fraction of the initial volume as an undiluted head at the end of a relatively short slumping distance, which then entrains ambient fluid as it proceeds downstream. Conversely, a high initial aspect ratio flow with the same initial volume has a component which remains essentially undiluted for a much longer distance to x_s, where a relatively smaller volume head emerges. As x_o/h_o or r_o/h_o increase, a behaviour approximating constant-flux release is approached, and some undiluted fluid can potentially reach great distances. To illustrate this point, figure 15 depicts

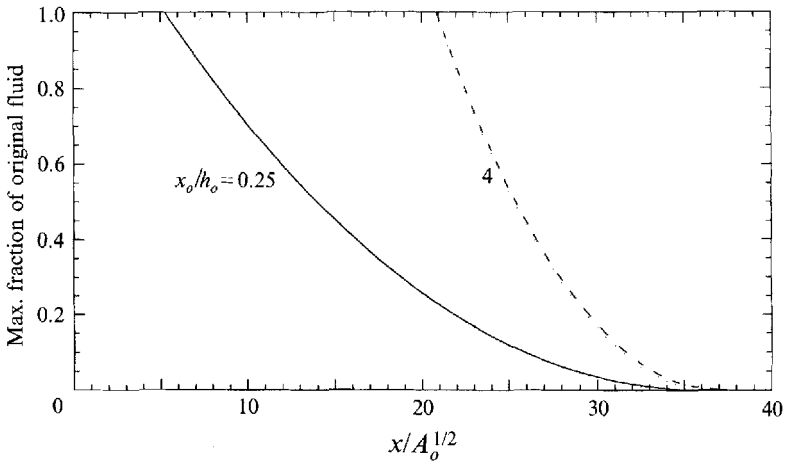

FIGURE 15. Maximum concentration expressed as a fraction of the initial concentration $(1/(1+E))$ plotted against normalized distance from the source for two gravity currents with identical initial volumes but different initial aspect ratios (x_o/h_o). Data evaluated using (3.14) with $S = (2/\pi)^{1/2}$, $\alpha = 0.063$ and $k = 0.127$.

the predicted dilution at the foremost point of two constant-volume-release gravity currents with identical initial volumes but different initial aspect ratios, measured with respect to normalized distance from the release point. It can be seen that the maximum concentration witnessed at given distances can vary quite markedly between the two cases.

Many natural and industrial flows are initiated with widely different aspect ratios, for example the collapse of tall, vertical volcanic eruption columns (low x_o/h_o), and the storm-generated suspension of sediment over wide areas in shallow seas (high x_o/h_o). For flows where the slumping distance is very much shorter than the final length of the turbulent flow, this effect may be irrelevant. However, for flows that achieve final lengths only a few multiples of the slumping distance, properties and behaviour that depend on dilution, such as sedimentation of particles, toxicity and chemical precipitation, will be strongly influenced by the release configuration.

We see then that the entrainment of ambient fluid into turbulent gravity currents is not as straightforward as conventional self-similar solutions describing their dynamics might suggest, and special consideration must be given to the spatially non-uniform character of entrainment into constant-volume-release flows.

We conclude that entrainment into the head of two-dimensional and axisymmetric fixed-volume gravity currents moving along a horizontal rigid boundary is well described using a general entrainment coefficient of $\alpha = 0.063 \pm 0.003$. The amount of entrainment at any given distance from the source beyond the slumping phase then depends on a relevant lengthscale of the head, which is some function of the volume of the head at that distance. We propose that the lengthscale applicable to these particular flows is the height of the head, and employ a shape factor S to relate the height of the head to its cross-sectional area. The shape factor depends on the frictional drag imposed at the base of the current, but is usefully approximated by $S = (2/\pi)^{1/2}$ for flows over a solid boundary. The volume of the head at any point beyond the slumping phase depends on the loss of original volume to the tail during that phase, which is in turn a function of the initial aspect ratio at release.

Our neutralization method has proved to be successful for directly measuring the

entrainment into constant-volume gravity currents, and although the technique could not be applied quantitatively to constant-flux currents, it remains useful for the qualitative elucidation of mixing dynamics.

We thank Brian Dade and Jim Rottman for interesting discussions on the material of this paper, and Charlotte Gladstone for conducting several experiments in the constant-flux regime. This research is partially supported by grants from the NERC.

REFERENCES

BEGHIN, P., HOPFINGER, E. J. & BRITTER, R. E. 1981 Gravitational convection from instantaneous sources on inclined boundaries. *J. Fluid Mech.* **107**, 407–422.

BENJAMIN, T. B. 1968 Gravity currents and related phenomena. *J. Fluid Mech.* **31**, 209–248.

BONNECAZE, R. T., HUPPERT, H. E. & LISTER, J. R. 1993 Particle-driven gravity currents. *J. Fluid Mech.* **250**, 339–369.

BREIDENTHAL, R. 1981 Structure in turbulent mixing layers and wakes using a chemical reaction. *J. Fluid Mech.* **109**, 1–24.

BRITTER, R. E. & SIMPSON, J. E. 1978 Experiments on the dynamics of a gravity current head. *J. Fluid Mech.* **88**, 223–240.

CHEN, J. C. 1980 Studies on gravitational spreading currents. PhD thesis, California Institute of Technology.

CORCOS, G. M. & Sherman, F. S. 1976 Vorticity concentrations and the dynamics of unstable free shear layers. *J. Fluid Mech.* **73**, 241–264.

CORCOS, G. M. & Sherman, F. S. 1984 The mixing layer: deterministic models of a turbulent flow. Part 1. Introduction and the two-dimensional flow. *J. Fluid Mech.* **139**, 29–65.

FANNELOP, T. K. & WALDMAN, G. D. 1972 Dynamics of oil slicks. *AIAA J.* **10**, 506–510.

FISCHER, H. B., LIST, E. J., KOH, R. C. Y., IMBERGER, J. & BROOKS, N. H. 1979 *Mixing in Inland and Coastal Waters.* Academic.

HALLWORTH, M. A., PHILLIPS, J. C., HUPPERT, H. E. & SPARKS, R. S. J. 1993 Entrainment in turbulent gravity currents. *Nature* **362**, 829–831.

HOULT, D. P. 1972 Oil spreading on the sea. *Ann. Rev. Fluid Mech.* **4**, 341–368.

HUPPERT, H. E. & SIMPSON, J. E. 1980 The slumping of gravity currents. *J. Fluid Mech.* **99**, 785–799.

JOHARI, H. 1992 Mixing in thermals with and without buoyancy reversals. *J. Atmos. Sci.* **49**, 1412–1426.

KÁRMÁN, T. VON 1940 The engineer grapples with nonlinear problems. *Bull. Am. Math. Soc.* **46**, 615–683.

KOOCHESFAHANI, M. M. & DIMOTAKIS, P. E. 1986 Mixing and chemical reactions in a turbulent liquid mixing layer. *J. Fluid Mech.* **170**, 83–112.

MORTON, B. R., TAYLOR, G. I. & TURNER, J. S. 1956 Turbulent gravitational convection from maintained and instantaneous sources. *Proc. R. Soc. Lond.* A **234**, 1–23.

ROTTMAN, J. W. & SIMPSON, J. E. 1983 The initial development of gravity currents from fixed-volume releases of heavy fluids. *J. Fluid Mech.* **135**, 95–110.

SIMPSON, J. E. 1987 *Gravity Currents in the Environment and the Laboratory.* Halsted Press, Chichester.

TURNER, J. S. 1986 Turbulent entrainment: the development of the entrainment assumption, and its application to geophysical flows. *J. Fluid Mech.* **173**, 431–471.